RESEARCH ARTICLE

"Dry gets drier, wet gets wetter": A case study over the arid regions of central Asia

Zengyun Hu[1,2] | Xi Chen[1] | Deliang Chen[3] | Jianfeng Li[2] | Shuo Wang[4] |
Qiming Zhou[2] | Gang Yin[5] | Meiyu Guo[2]

[1]State Key Laboratory of Desert and Oasis Ecology, Xinjiang Institute of Ecology and Geography, Chinese Academy of Sciences, Urumqi, China

[2]Department of Geography, Hong Kong Baptist University, Hong Kong, China

[3]Department of Earth Sciences, University of Gothenburg, Gothenburg, Sweden

[4]Department of Land Surveying and Geo-informatics, The Hong Kong Polytechnic University, Hong Kong, China

[5]College of Information Science & Engineering, Xinjiang University, Urumuqi, China

Correspondence
Qiming Zhou, Department of Geography, Hong Kong Baptist University, Kowloon, Hong Kong, China.
Email: qiming@hkbu.edu.hk

The "dry gets drier, wet gets wetter" (DGDWGW) paradigm well describes the pattern of precipitation changes over the oceans. However, it has also been usually considered as a simplified pattern of regional changes in wet/dry under global warming, although GCMs mostly do not agree this pattern over land. To examine the validity of this paradigm over land and evaluate how usage of drought indices estimated from different hydrological variables affects detection of regional wet/dry trends, we take the arid regions of central Asia as a case study area and estimate the drying and wetting trends during the period of 1950–2015 based on multiple drought indices. These indices include the standardized precipitation index (SPI), the standardized precipitation evapotranspiration index (SPEI), the Palmer drought severity index (PDSI) and self-calibrating PDSI (sc_PDSI) with both the Thornthwaite (th) and Penman–Monteith (pm) equations in PDSI calculation (namely, PDSI_th, PDSI_pm, sc_PDSI_th and sc_PDSI_pm). The results show that there is an overall agreement among the indices in terms of inter-annual variation, especially for the PDSIs. All drought indices except SPI show a drying trend over the five states of central Asia (CAS5: including Kazakhstan, Kyrgyzstan, Tajikistan, Turkmenistan and Uzbekistan). The four PDSIs and SPEI reveal a wetting tendency over the northwestern China (NW; including Xinjiang Uygur Autonomous Region and Hexi Corridor). The contrasting trends between CAS5 and NW can also be revealed in soil moisture (SM) variations. The nonlinear wet and dry variations are dominated by the 3–7 years oscillations for the indices. Relationships between the six indices and climate variables show the major drought drivers have regional features: with mean temperature (TMP), precipitation total (PRE) and potential evapotranspiration (PET) for CAS5, and PRE and PET for NW. Finally, our analyses indicate that the dry and wet variations are strongly correlated with the El Niño/Southern Oscillation (ENSO).

KEYWORDS
central Asia, dry and wet, SPI, SPEI, PDSI

1 | INTRODUCTION

Global climate change has resulted in changes of drought conditions in arid regions around the world (e.g., Chen and Chen, 2013). Assessment of wetting and drying trends has been becoming one of the most significant scientific issues because the wet and dry variations can induce droughts and floods which have devastating impacts on regional water resources, agriculture and the environment, with far-reaching implications for human society (Sheffield et al., 2012; Lesk et al., 2016). In many cases, the "dry gets drier, wet gets wetter" (DGDWGW) paradigm has been recognized as a simplified summary of the impacts of global warming on regional trends in wetting/drying, although many studies have demonstrated that this paradigm is mostly valid in oceanic data (Allan et al., 2010; Chou et al., 2013). For example, Greve et al. (2014) indicated that only 10.8% of the global land area follows robust patterns of DGDWGW. On

the other hand, regional changes in wetting/drying trends estimated from different hydrological variables may generate contradicting results, which introduces further uncertainties to the validity of the DGDWGW paradigm. In fact, most of previous studies mainly used precipitation only to characterize the regional wetting/drying trends, but precipitation change alone cannot fully reveal changes in wet/dry conditions, and therefore other climatic and hydrological variables should be considered as well, such as evapotranspiration (E) or potential evapotranspiration (PET) and soil moisture (SM; Hu and Huang, 2009; Greve et al., 2014; Feng and Zhang, 2015). As some previous analyses (Greve et al., 2014; Feng and Zhang, 2015) pointed out, aridity over land has not followed a simple intensification of DGDWGW, and the global drought has been overestimated. Therefore, the regional changes in dry and wet conditions should be assessed based on different climatic and hydrological factors (Greve et al., 2014).

In recent years, a number of indices have been developed and widely applied to estimate dry and wet events and evaluate their developments (Wells et al., 2004; Vicente-Serrano et al., 2010; Dai, 2011a). As one of the most commonly used drought indices, the Palmer drought severity index (PDSI; Palmer, 1965) is based on the supply and demand of a water balance equation (i.e., a two-layer bucket-type model for soil moisture calculations) which enables measurement of both wetness (positive value) and dryness (negative value). In the calculation of PDSI, there are two approaches to estimate PET: (a) the Thornthwaite equation (Thornthwaite, 1948) which is based only on daily averaged temperatures and latitude and (b) the Penman–Monteith equation (Palmer, 1965) which is more physically based parameterizations of PET by additional input fields including wind speed, solar radiation, temperature and water vapour content. The corresponding PDSI are named PDSI_th and PDSI_pm. Although PDSI_th could lead to errors in energy-limited regions (Hobbins et al., 2008), both PDSI_th and PDSI_pm are very similar in terms of temporal correlation, regional averages and trends in several regions (e.g., Australia, central North America and central Asia) because of the same water balance model (Schrier et al., 2011). To address the problem of spatial incomparability of PDSI, Wells et al. (2004) proposed a self-calibrating PDSI (sc_PDSI) by calibrating the PDSI using local conditions, instead of using the (fixed) coefficients used by Palmer (1965) based on data from the central United States, and the sc_PDSI with the PET based on Thornthwaite equation and Penman–Monteith equation are noted as sc_PDSI_th and sc_PDSI_pm, respectively. The PDSI is generally considered as a meteorological drought index and can also be used for agricultural drought characterizations (Hao and Singh, 2015). It is important to keep in mind though that PDSI has a fixed temporal scale (between 9 and 12 months) and a strong memory which can vary from

place to place (Guttman, 1998; Vicente-Serrano et al., 2010).

With the advantage of being multiscale, SPI based on a precipitation probabilistic approach (McKee et al., 1993) and SPEI based on precipitation and PET determined by temperature data (Vicente-Serrano et al., 2010) have been widely used to detect the dry and wet variations (Chen et al., 2017). The major difference between the two indices is that SPI only includes precipitation (Hao and Singh, 2015), while SPEI considers the difference between precipitation and PET (Vicente-Serrano et al., 2010). PDSI has even more sophisticated treatment of water balances. It should be noted that changes in ET can be different from that in PET. As an example, in moisture stressed areas (e.g., arid area), the PET usually increases whereas the E decreases (Zhang et al., 2017). The PDSI considers ET in the water balance and the SPEI uses PET which makes that droughts are amplified in the SPEI in comparison to PDSI (or SPI) (Hao and Singh, 2015). However, more complex methods also require more inputs, which can add additional uncertainties if the input variables are not accurate. Besides, different indices focus on different aspects of dry/wet conditions. Consequently, multiple drought indices should be considered to evaluate the wet and dry conditions comprehensively.

As the largest arid area in the temperate and warm temperate regions of the Northern Hemisphere, the arid regions of central Asia (CASNW: including the five states of central Asia [CAS5: Kazakhstan, Kyrgyzstan, Tajikistan, Turkmenistan and Uzbekistan] and northwestern China [NW]) have very sensitive and vulnerable ecosystem to the arid and semiarid climate (Chen, 2012). However, as in situ observations are scarce and limited in time and space, there are few studies about the climate variations (Hu et al., 2014; Hu et al., 2016a; 2016b). In the last century, the CASNW have experienced a larger warming trend than its surrounding areas, especially in recent three decades (Hu et al., 2014). Although there is no significant increasing trend for the precipitation over the whole region, contrasting regional trends have been identified, that is, a decreasing trend in CAS5 and an increasing trend in NW during the period of 1951–2013 (Hu et al., 2017). Therefore, changes in wet and dry conditions in the study region with consideration of precipitation, temperature, and other climatic variables are not well known. For instance, the concept of DGDWGW has been verified over the ocean, but not hold over the global lands (Greve et al., 2014). Therefore, whether this pattern is valid over the arid regions of central Asia should be further studied.

As one of the important drivers of internal variability in climate, El Niño/Southern Oscillation (ENSO) has great effects on the wet and dry variations around the world through the ocean–atmosphere interactions (Nicholson et al., 2001; Hu and Huang, 2009; Vicente-Serrano et al., 2011; Dai, 2011a; Trenberth et al., 2014). Furthermore, previous

studies (Mariotti, 2007; Hu *et al.*, 2017) have indicated that ENSO affects the variations and magnitude of precipitation over the arid regions of central Asia, although the exact extent to which the wet and dry variations over the arid regions of CASNW are dependent on ENSO remains to be determined. If a close relationship can be established, it may provide some potential for forecasting the wet and dry events as the predictability of ENSO is high.

To address the above questions, we apply multiple drought indices including SPI, SPEI and the four PDSIs (PDSI_th, PDSI_pm, sc_PDSI_th and sc_PDSI_pm) to identify the dry and wet variations over CASNW and their relationship with ENSO. The paper is organized as follows: in section 2, the study area, data and the methodologies are briefly described. The results are provided in section 3. The discussion is shown in section 4. The last section summarizes conclusions.

2 | STUDY AREA, DATA SETS AND METHODOLOGY
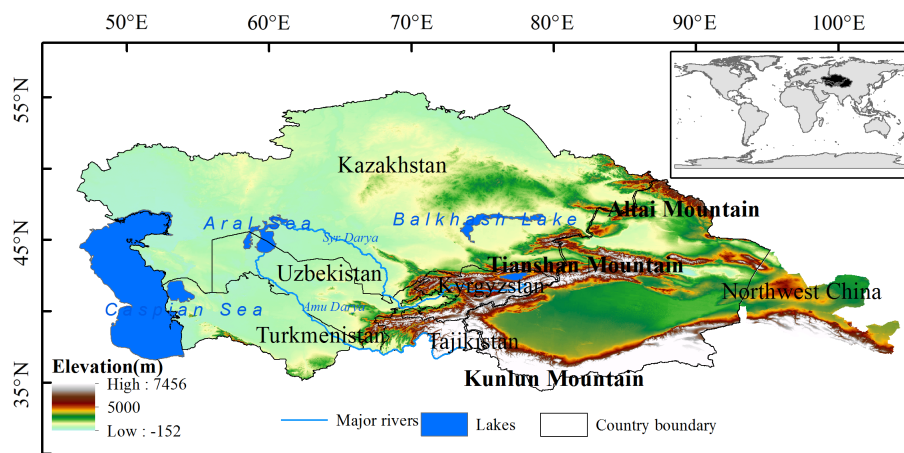
2.1 | Study area

The CASNW consists of CAS5 and NW covering more than 6×10^6 km^2 (Figure 1) (Chen, 2012; Chen and Zhou, 2015). In the west, it adjoins the Caspian Sea; in the south, it includes the Amu Darya Basin; its northern area reaches to the Irtysh River basin in Kazakhstan and China, and it includes the Heixi Corridor. Therefore, it is the core area of the Silk Road Economic Zone. This region is located in the hinterland of the Eurasian continent with complex terrain and geomorphic features. It includes the major mountains: the Altai, Tianshan, Kunlunand Qilian Mountains; its major lakes and rivers include the Aral Sea, Balkhash Lake, Issyk-Kul Lake, Syr Darya, Amu Darya and Tarim River (Figure 1).

Because of its special geographical location and complex topography, this region is dominated by an arid and semiarid climate which is primarily controlled by the westerly winds (Lioubimtseva and Cole, 2006; Chen and Zhou, 2015). The Atlantic Ocean and the Arctic Ocean provide the most moisture fluxes to the regions, while the moisture fluxes from the Pacific Ocean and the Indian Ocean are mostly hindered by the Tianshan Mountain and the Pamirs (Schiemann *et al.*, 2008). During El Niño, part of the moisture fluxes originated from the Indian Ocean are carried by the westerly wind to strengthen the precipitation over the most parts of central Asia, especially the middle southern region (Mariotti, 2007; Hu *et al.*, 2017). The annual precipitation over the region is less than 150 mm on average, with significant spatial differences: more precipitation over the mountainous areas than that of the plain areas (Chen, 2012; Hu *et al.*, 2017).

2.2 | Data sets

Three types of commonly used meteorological drought indices, including SPI, SPEI and PDSI, are used in this study. For PDSI, we adopt four different varieties of PDSI, namely PDSI_pm, sc_PDSI_pm, PDSI_th and sc_PDSI_th, which are based on the same calculation framework but different algorithms for PET and calibration. Although SPI can provide different timescales (e.g., 1, 3, 6, 9, 12 months) to reveal the characteristics of dry and wet, in order to have a comparison with the other indices, all the drought indices have a unified annual timescale (12-month scale for SPI and SPEI). The other timescales of SPI and SPEI are not considered in this study. Three climatic variables: mean temperature (TMP), precipitation total (PRE) and PET are used to identify the major drivers of drought. To further understand the changes of dry and wet, SM is also applied in this study.

In central Asia, the meteorological stations are sparse and highly unevenly distributed which only provide limited observed records. Especially most stations outside China stopped functioning in the 1990s after the dissolution of the

FIGURE 1 Study area and its topography, including the major rivers: Syr Darya and Amu Darya, the major mountains: the Tianshan Mountain, Kunlun Mountain and Altai Mountains [Colour figure can be viewed at wileyonlinelibrary.com]

TABLE 1 Data sets used in this study

Data set	Acronym	Temporal resolution	Spatial resolution	Source/references
Mean temperature	TMP	1901–2015 (monthly)	0.5° × 0.5°	Harris *et al*. (2014) CRUTS v4.0, https://crudata.uea.ac.uk/cru/data/hrg/cru_ts_4.00/cruts.1701270849.v4.00/
Precipitation total	PRE	1901–2015 (monthly)	0.5 × 0.5°	PET is calculated from a variant of the Penman–Monteith formula
Potential evapotranspiration	PET	1901–2015 (monthly)	0.5° × 0.5°	
Standardized precipitation index	SPI	1901–2015 (monthly)	0.5 × 0.5°	Computed from PRE
Standardized precipitation evapotranspiration index	SPEI	1901–2015 (monthly)	0.5 × 0.5°	Computed from PRE and PET
Palmer drought severity index Penman–Monteith	PDSI_pm	1948–2012 (monthly)	1 × 1°	Sheffield *et al*. (2012), http://hydrology.princeton.edu/data/pdsi/
Self-calibrated PDSI_pm	sc_PDSI_pm	1948–2012 (monthly)	1 × 1°	
Palmer drought severity index Thornthwaite	PDSI_th	1948–2012 (monthly)	1 × 1°	
Self-calibrated PDSI_th	sc_PDSI_th	1948–2012 (monthly)	1 × 1°	
Soil moisture	SM	1948–present (monthly)	0.5 × 0.5°	Fan and Dool (2004), provided by the Earth System Research Laboratory of National Oceanic and Atmospheric Administration (NOAA) https://www.esrl.noaa.gov/psd/data/gridded/data.cpcsoil.html
El Niño–Southern Oscillation index	ENSO	1950–preseent (monthly)		From the Climate Prediction Center of NOAA, http://www.cpc.ncep.noaa.gov/data/indices/ersst4.nino.mth.81-10.ascii, Niño3.4 (5°N–0.5°S, 120°–170°W)

former Soviet Union, causing discontinuation of meteorological data for analysis of regional climate variations in the recent decades (Schiemann *et al*., 2008; Hu *et al*., 2014). Therefore, it is practically difficult to use observations of meteorological variables (e.g., precipitation, temperature, radiative variables, near-surface wind and SM) with acceptable length and quality to compute the drought indices. Recent studies show that temperature and precipitation data sets from CRU have the capability to reasonably represent the changes and variations of the temperature and precipitation over central Asia (Hu *et al*., 2014; Hu *et al*., 2018). Therefore, in this study, TMP, PRE and PET with the spatial resolution 0.5 × 0.5° and the period of 1901–2015 are from the latest version of the Climatic Research Unit time series (CRUTS v4.0) (Harris *et al*., 2014) (Table 1). The PET data set of CRU is derived from 0.5 × 0.5° gridded absolute values of TMP, minimum temperature (TMN), maximum temperature (TMX), vapour pressure (VAP) and cloud cover (CLD), and from a fixed monthly climatology for wind speed using a variant of the Penman–Monteith method (Harris *et al*., 2014). The gridded TMP, TMN, TMX, VAP and CLD data sets are interpolated from the meteorological stations which are processed by the strict quality control. Therefore, it is reasonable to compute the SPI and SPEI based on PRE and PET from CRU as previous studies (Sheffield *et al*., 2012; Trenberth *et al*., 2014; Li *et al*., 2017). The 12-month scale SPI and SPEI are used here for long-term analysis. Four types of PDSIs (PDSI_pm, sc_PDSI_pm, PDSI_th and sc_PDSI_th) are obtained from Princeton University with the spatial resolution 1 × 1° and the period of 1948–2012 (Sheffield *et al*., 2012).

SM plays an important role in environmental processes through its influence on water and energy exchanges between the land surface and atmosphere (Seneviratne *et al*., 2010; Cheng and Huang, 2016). Its variability can reveal the

dryness and wetness of the ground directly and help to understand the climate change indirectly (Seneviratne *et al*., 2010). Previous studies (Dai *et al*., 2004; Sheffield and Wood, 2008; Wang *et al*., 2015) have applied SM as an agricultural drought indicator and compared it with the other drought indices. Therefore, the estimated SM data are used for a comparison with the drought indices for a further analysis of the dry and wet variations. The SM data set at 0.5° resolution from 1948 to present is developed by 1-layer "bucket" water balance model with its depth layer of 1.6 m and provided by the Climate Prediction Center (CPC) of the Earth System Research Laboratory of National Oceanic and Atmospheric Administration (NOAA) (Table 1). Although this SM data set is the output from a water balance model, this data set is reasonably good against the limited observations in both the simulated annual cycle and inter-annual variability of soil moisture over different regions (Fan and Dool, 2004).

In this study, ENSO is indicated by Niño3.4 index which is obtained from the CPC of NOAA with the period of 1950 to present (Table 1). The details of the above data sets can be found in Table 1. We should note that all the data sets are analysed at annual scale obtained from their monthly scales. The study periods are 1950–2015 for SPI and SPEI, and 1950–2012 for the four PDSIs. All the other data sets are resampled on the same spatial resolution 1 × 1° of PDSI data sets by the bilinear interpolation method.

2.3 | Methodology

2.3.1 | Linear trend and ensemble empirical mode decomposition method

The linear trend k obtained by the linear least square method is used to quantify the tendency of the drought index during the periods of 1950–2012 for all the six indices during

1950–2015. The Student's *t* test is used to examine whether the linear trend *k* is statistically significant at the 95% confidence level ($p < .05$) and 99% confidence level ($p < .01$).

In order to extract the multi-period characteristics of the six drought indices, the ensemble empirical mode decomposition (EEMD) method is applied (Wu and Huang, 2009; Ji *et al.*, 2014). EEMD is an adaptive time–frequency data analysis method which can extract signals from data generated in noisy nonlinear and nonstationary processes (Wu and Huang, 2009). In addition, it overcomes the scale separation problem without introducing a subjective intermittence test. Therefore, the EEMD method has been demonstrated to be a powerful tool to analyse nonlinear and nonstationary data in climate, hydrology and ecosystem (Qian *et al.*, 2011; Franzke, 2012; Yin *et al.*, 2017). It has the capability and the advantage in extracting the annual cycle component from a climate variable have been validated through analysing synthetic data and monthly sea surface temperature data (Qian *et al.*, 2011).

For a time series $\{x(t)\}$, a white noise $w(t)$ with finite amplitude is added, we have

$$X(t) = x(t) + w(t). \tag{1}$$

Then, $X(t)$ is decomposed in the intrinsic mode functions (IMFs) c_j

$$X(t) = \sum_{j=1}^{n} c_j(t) + r_n(t), \tag{2}$$

where r_n is the residue of data $X(t)$, after *n* number of IMFs are extracted. At last, we can obtain the IMFs with different periods which are also the periods of the time series $x(t)$. The residue term *r* reflects the nonlinear trend based on the EEMD method (Ji *et al.*, 2014). The added white noise $w(t)$ in each EEMD ensemble member has a standard deviation (*SD*) of 0.2 and an ensemble size of 100 is used. The significance of the periodicity for each EEMD component is detected at the 95% confidence level (Wu and Huang, 2004). The detailed description of the EEMD method can be found in Wu and Huang (2009).

2.3.2 | Correlation coefficient

Correlation coefficient (CC) values are used to measure the strength and direction of the linear association between two time series. In this study, CC values are computed between the six drought indices to identify the linear correlations between them. The influences of the climate factors (i.e., TMP, PRE and PET) on the drought indices are also quantified by the CC values. In order to compare the relationships among the drought indices and SM, the CC values are also used. Further, the correlations between the drought indices and ENSO are analysed based on the CC values to quantify the impact of ENSO on the wet and dry variations over the arid regions of central Asia.

3 | RESULT

3.1 | Temporal variations of the drought indices during 1950–2015

3.1.1 | Linear trends of the six drought indices

For the entire study area (CASNW), SPI and SPEI have similar inter-annual variations except the large difference after 2003, which results in the significantly positive linear trend ($k = 0.006$/year, $p < .05$) for SPI and the significantly negative linear trend ($k = -0.01$, $p < .01$) for SPEI during 1950–2015 (Figure 2a and Table 2). The large difference seems to be caused by the increased PET after 2003 which is considered in SPEI but not in SPI. This difference shows the importance of PET in the later period, indicating that precipitation alone is not enough to describe drying/wetting trend in CASNW under climate change.

In terms of the four PDSIs, they have highly consistent variabilities for the whole study period (Figure 2b) with the CC values larger than 0.85 (Table 3). All the four PDSIs show drying linear trends as SPEI although they are not statistically significant (Table 2). Further, the five drought indices have the largest values in 1993 except PDSI_pm in 2003. For the smallest value years, SPI and PDSI_pm appear in 1975, the other three PDSIs are in 1997, and SPEI is in 2008. The averaged CC value between SPI (SPEI) and the four PDSIs is larger than 0.82 (0.85), which shows the six drought indices have similar inter-annual variations. It should be noted that the variations between SPEI and the four PDSIs are more similar than those between SPI and PDSIs (Table 3), which is not surprising as SPI only considers precipitation.

For CAS5, SPI displays a slight wetting trend, while the other five drought indices show drying. This again shows that the combined climate change effect, in contrast to precipitation change alone, should be considered in describing changes in drought (Figure 2c,d and Table 2). In particular, the drying trends of SPEI and sc_PDSI_th are significant at the 95% confidence level (Table 2). Compared with CAS5, NW has the wet tendency according to the increasing trends of the drought indices (except the decreasing trend of SPEI) during the period of 1950–2015. Specifically, the sc_PDSI_th has the largest positive trend ($k = 0.015$/year, $p < .05$ for 1950–2012) among the six drought indices, followed by SPI ($k = 0.012$/year, $p < .01$ for 1950–2015) (Table 2). To explore the possible reasons about the opposite trends between PDSI and SPEI in NW, the temporal variation of SM is displayed in Figure S1, Supporting Information. NW has a significant increasing trend of SM during the period of 1950–2015 which contributes to the positive trend of PDSI. On the other hand, since SPEI only considers the differences of PRE and PET, PET is expected to increase due to increasing TMP of NW, resulting in decreasing SPEI. Furthermore, Figure S1 also shows the negative trends of the
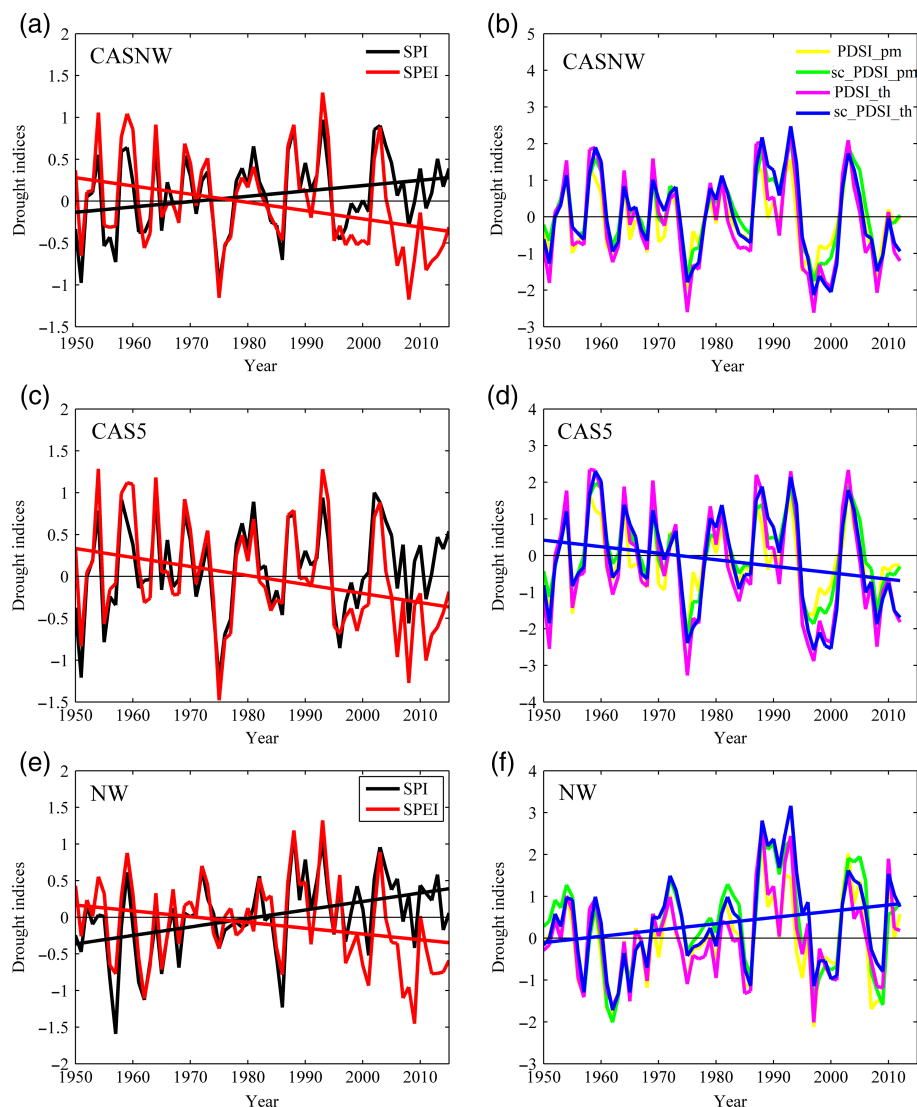
FIGURE 2   Temporal variations of the annual drought indices over CASNW, CAS5 and NE during 1950–2015, where the linear trend lines are only for the drought indices with significant linear trend at the 95% confidence level ($p < .05$) [Colour figure can be viewed at wileyonlinelibrary.com]

PDSI in CAS5 are influenced by the decreasing trend of SM.

It is interesting that SPI and SPEI have the obviously opposite trends over both CASNW and NW (Figure 2a,e). In fact, from 1950 to the mid-1990s, SPI and SPEI have the same variabilities with small differences. After 1995, the differences become significantly large (i.e., SPEI is much smaller than SPI) which cause the opposite trends between SPI and SPEI over CASNW and NW during the whole period of 1950–2015. In CAS5, SPEI is also much smaller than SPI from 1995 to 2015. This can be understood that all the three regions have the equivalent warming trends in TMP with the rate of 0.3 °C/10 years during 1950–2015 (Figure 3a), non-significant increasing trends in PRE are found for CASNW and CAS5 and significant increasing trend of PRE over NW (Figure 3b). For PET, the three regions all have the significantly increasing trends with the rate of 0.93, 1.07 and 0.63 mm/year for CASNW, CAS5 and NW, respectively

(Figure 3c). Moreover, the PET has a remarkable increase over the three regions during 1995–2015. The trends in the period of 1995–2015: 1.93, 2.03 and 1.7 mm/year for CASNW, CAS5 and NW are at least two times than the corresponding trends in the whole period. Due to the large increase in PET during 1995–2015, SPI and SPEI have the opposite trends in the whole period. The significantly increasing trend in PRE over NW results in the wetting trend, whereas the drying trend over CAS5 may be caused by the significantly increasing trend in PET. The major factors among TMP, PRE and PET to the wet and dry variations over the three regions will be detected by the CC values in the following section. The wet events (e.g., maximum drought indices) appear at 1950s (SPEI, sc_PDSI_pm, PDSI_th and sc_PDSI_th) and the early 2000s (SPI and PDSI_pm) over CAS5, at 1988 (SPI, PDSI_pm, sc_PDSI_pm and PDSI_th) and 1993 (SPEI and sc_PDSI_th) over NW. All the drought indices have the dry

TABLE 2 Linear trend (index value per year), maximum drought indices, minimum drought indices and the corresponding years during 1950–2015.
* means that the trends are statistically significant at the 95% level ($p < 0.01$), ** significant at the 99% level ($p < 0.01$) with the Student's t test

Study area	Drought index	k	MAX	MAX-Y	MIN	MIN-Y
CASNW	SPI	0.006*	0.97	1993	−0.99	1975
	SPEI	−0.01**	1.30	1993	−1.18	2008
	PDSI_pm	−0.001	1.96	2003	−1.99	1975
	sc_PDSI_pm	−0.003	2.07	1993	−1.75	1997
	PDSI_th	−0.010	2.36	1993	−2.62	1997
	sc_PDSI_th	−0.008	2.47	1993	−2.14	1997
CAS5	SPI	0.004	1.00	2002	−1.24	1975
	SPEI	−0.011**	1.28	1954	−1.48	1975
	PDSI_pm	−0.005	1.94	2003	−2.41	1975
	sc_PDSI_pm	−0.009	1.98	1959	−2.22	1975
	PDSI_th	−0.018	2.35	1958	−3.28	1975
	sc_PDSI_th	−0.018*	2.30	1959	−2.58	1997
NW	SPI	0.012**	1.15	1988	−1.59	1957
	SPEI	−0.008*	1.32	1993	−1.45	2009
	PDSI_pm	0.007	2.28	1988	−2.12	1997
	sc_PDSI_pm	0.010	2.65	1988	−2.01	1962
	PDSI_th	0.008	2.69	1988	−2.01	1997
	sc_PDSI_th	0.015*	3.16	1993	−1.72	1962

TABLE 3 Correlation coefficient (CC) between the annual drought indices over the entire study area (CASNW) during 1950–2015. All the CC values are significant at the 99% confidence level

| Drought indices	SPI	SPEI	PDSI_pm	sc_PDSI_pm	PDSI_th	sc_PDSI_th
SPI	1.00	0.72	0.85	0.81	0.85	0.79
SPEI		1.00	0.82	0.83	0.91	0.87
PDSI_pm			1.00	0.92	0.93	0.85
sc_PDSI_pm				1.00	0.93	0.96
PDSI_th					1.00	0.95
sc_PDSI_th						1.00

event (e.g., minimum drought indices) year in 1975 over CAS5 except for sc_PDSI_th in 1997. However, there is not a same year for the drought indices over NW (Table 2). Although there are differences in the trends revealed by the six drought indices, they have broadly consistent temporal variations over CAS5 and NW according to the CC values (Table S1), especially for the CC values between the four PDSIs. Depending on region and climate conditions, SPI and SPEI can show different values/trends. They can also indicate different or similar trends compared with other four PDSIs, depending on the dominating climate conditions.

3.1.2 | Multi-periods and the nonlinear trends of the drought indices

In this section, the multi-periods and nonlinear trends of the six drought indices are explored by EEMD method which is used to detect whether they have the similar nonlinear characteristics. The decomposition results of the annual drought indices over CASNW during the period of 1950–2015 are displayed in Figure 4. The corresponding quasi-periods and nonlinear trends are provided in Table S2.

Figure 4a shows that each EEMD component of SPI has relatively stable quasi-period oscillations, with the mean periods of 3 years for c_1, 7 years for c_2, 13 years for c_3 and 29 years for c_4 (Table S2). The inter-annual timescale components totally explain 79.7% (38.3 and 41.3% for c_1 and c_2, respectively) variances of SPI, which indicates that the inter-annual signal is the dominant component of the SPI variability over CASNW. Further, the 7 years quasi-period is significant at the 95% confidence level. For SPEI, the inter-annual signals (c_1 and c_2) have similar oscillations as these of the SPI (Figure 3b) with the 3 year period for c_1 and 7 year period for c_2 (Table S2). With more than 81.0% contribution to the variances of SPEI (49.2% for c_1 and 32.3% for c_2), they are also the dominant components which are similar to SPI. The signs of the nonlinear trends of SPI and SPEI are same as the linear trends, with $r = 0.56$ for SPI and $r = -0.49$ for SPEI.

For the four PDSIs, the inter-annual signals have the 3–7 year periods and they are still the dominant components of the drought indices accounting for more than 70.0% variabilities (Figure 4c,f and Table S2). PDSI_pm and sc_PDSI_pm have the positive nonlinear trends with the
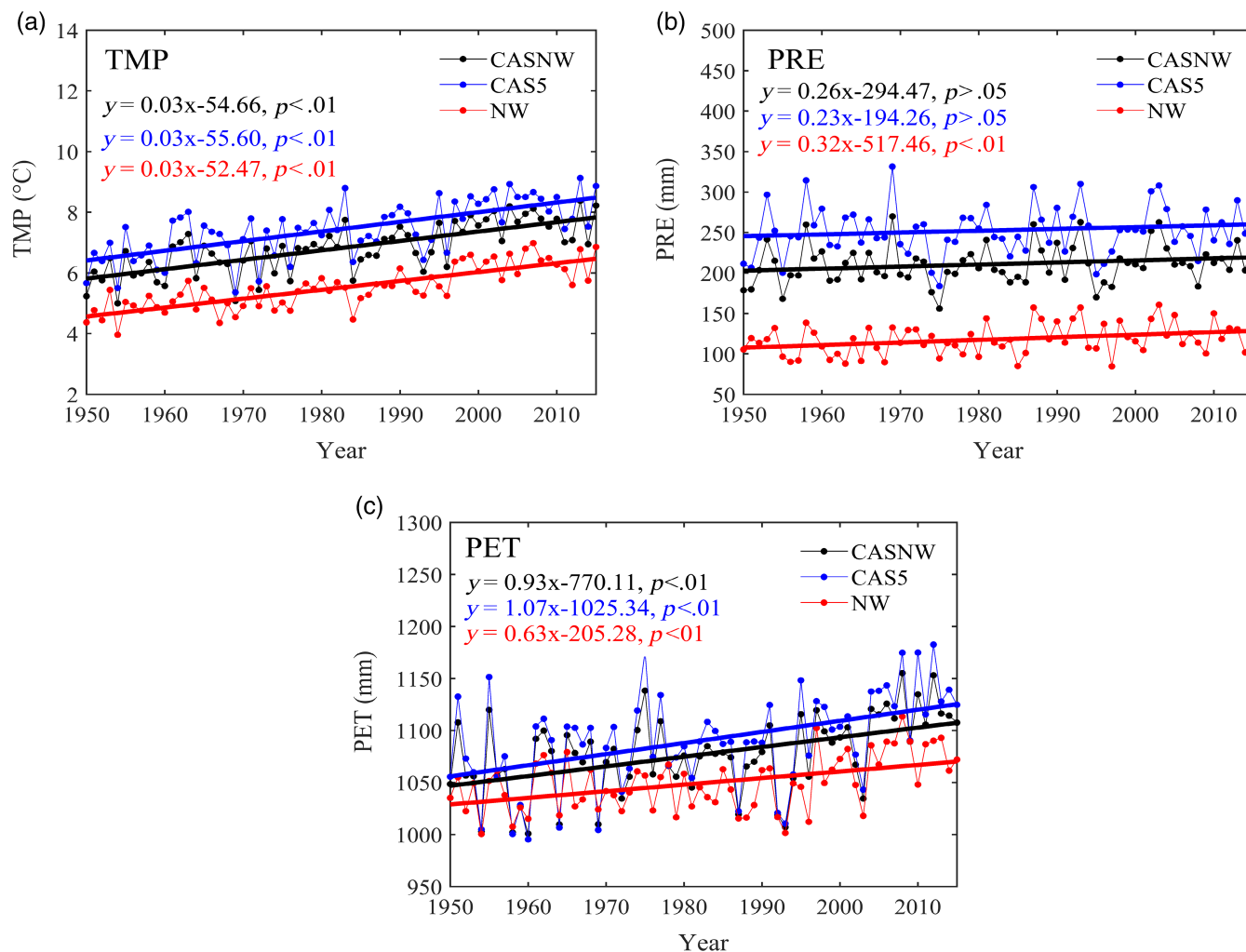
FIGURE 3 Temporal variations of the TMP (a), PRE (b) and PET(c) over CASNW (black colour), CAS5 (blue colour) and NE (red colour) during 1950–2015, where the dotted lines are the time series of TMP, PRE and PET, and the straight lines are the corresponding linear trend results obtained by the least squares method [Colour figure can be viewed at wileyonlinelibrary.com]

values of 0.21 and 0.28, respectively (Table S2) which are opposite to the corresponding linear trends in Table 2. The negative nonlinear trends are obtained for PDSI_th ($r = 0.25$) and sc_PDSI_th ($r = 0.24$) which have the same signs as their linear trends (Table S2).

For the EEMD result of the drought indices over CAS5 and NW (decomposition result figure not shown), the six drought indices have the low-frequency variations with 3–7 year quasi-periods which have more than 70.0% variation explanations (Table S2). Further, the quasi-periods of c_2 over CAS5 are significant at the 95% confidence level, with the periods of 6 years for sc_PDSI_th and 7 years for the other five PDSIs. From the nonlinear trends, CAS5 has the drought trend and NW has the wetting trend, which are again consistent with the linear trend results.

3.2 | Spatial characteristics of the six drought indices

The above analyses show that the six drought indices overall have similar temporal variabilities over CASNW, CAS5 and NW, with the drying tendency in CAS5 and the wetting

tendency in NW. In this section, we consider the spatial distribution of linear trends of the drought indices, which will help identify eventual common signal and possible reasons for any differences.

Figure 5 shows the spatial distributions of the linear trends of the six drought indices. The linear trends of SPI and SPEI have the opposite spatial distributions and the four PDSIs indices have the similar distributions over most of the entire study region (Figure 5). Specifically, SPI has the positive linear trends over most areas of CASNW with the centres in the northwest of Kazakhstan and western Uzbekistan, most of Xinjiang and south of Hexi Corridor (Figure 5a). For SPEI (Figure 5b), almost all of the CASNW have the negative linear trends with the centre areas at south-central of Kazakhstan, most of Uzbekistan and Turkmenistan, south-central of Xinjiang and north of Hexi Corridor. The four PDSIs show the opposite linear trends between CAS5 and NW with most positive trends occurring in Xinjiang and most negative trends detected over the southern Kazakhstan, Uzbekistan and Turkmenistan (Figure 5e,f). Further, because PDSI_th and sc_PDSI_th only used temperature
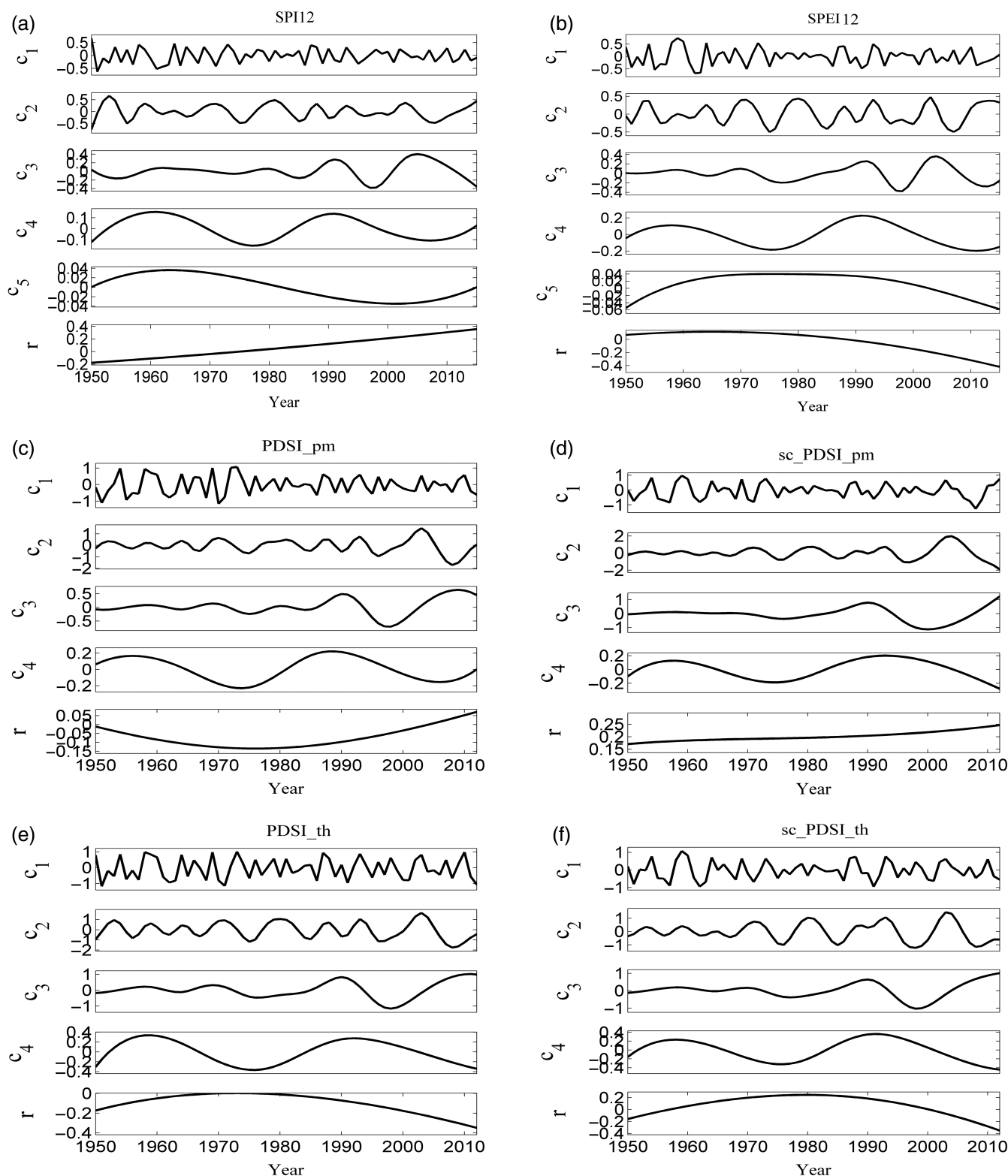
FIGURE 4 The decomposition results of the annual drought indices by EEMD method during 1950–2015

which has a significant warming trend in the PET computing, the negative areas of them are larger than these of PDSI_pm and sc_PDSI_pm. This analysis demonstrates that SPI and SPEI often show different signs of the regional trends, while the four PDSIs show a consistent regional distribution of the trends. The difference between the trends revealed by SPI and the PDSIs is much smaller than those

between SPEI and PDSIs. This may be caused by high uncertainty in estimating the PET. Previous studies have shown that PET estimate can be sensitive to certain input variables (e.g., Gong *et al.*, 2006) and different estimates can even produce opposite trends (Chen *et al.*, 2005).

Moreover, to help understand the spatial patterns of the linear trends of the drought indices, the spatial distributions
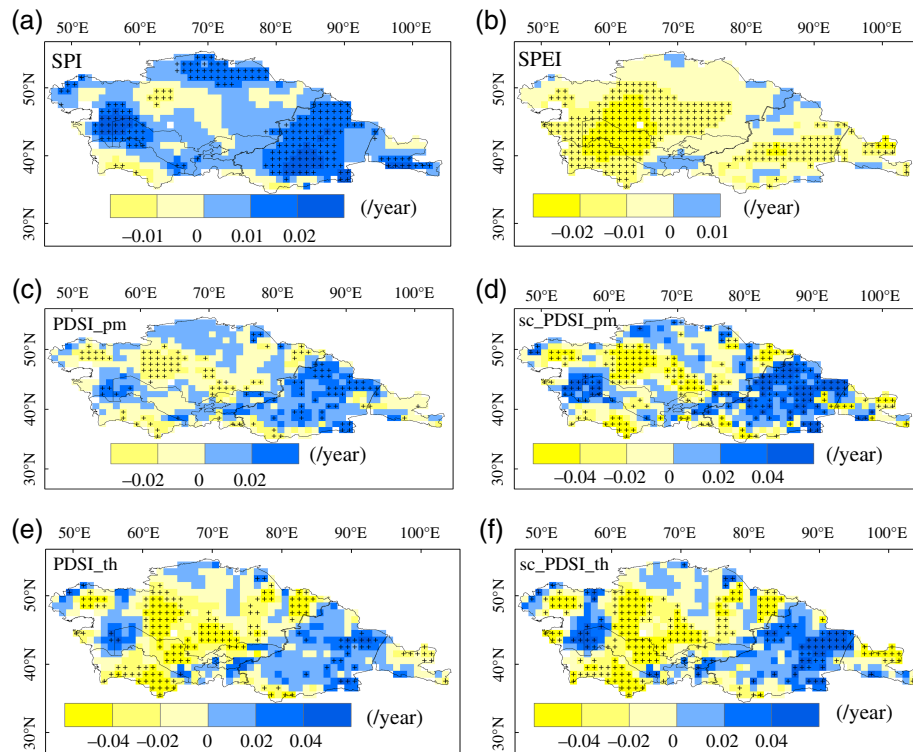
FIGURE 5 Spatial distributions of the linear trends of the annual drought indices, SPI (a) and SPEI (b) for 1950–2015, PDSI_pm (c), sc_PDSI_pm (d), PDSI_th (e) and sc_PDSI_th (f) for 1950–2012. Statistically significant linear trends at the 95% confidence level are indicated by cross ($p < .05$) [Colour figure can be viewed at wileyonlinelibrary.com]

of the long-term linear trends of TMP, PRE, PET and SM are displayed in Figure 6. Significantly positive trends of TMP are distributed over CASNW with the centre regions in western and northern Xinjiang, and Aral Sea which indicate the warming tendency during 1950–2015 (Figure 6a). The linear trends of PRE have regional differences with the positive trends areas mainly in part of the northern Kazakhstan, northwestern Uzbekistan, Tajikistan and western and northern Xinjiang, and the negative trends areas in part of central

Kazakhstan and most of Turkmenistan (Figure 6b). Under the warming temperature over CASNW, most regions have significantly positive trends at the 95% confidence level ($p < .05$), and the positive trend centres appear in southwestern CAS5 (Figure 6c). For SM, the spatial distributions are similar to these of drought indices with the positive trends mainly in northern Kazakhstan and most of NW, and the negative trends in central and southern CAS5 (Figure 6d). Furthermore, detailed analyses about the relationships
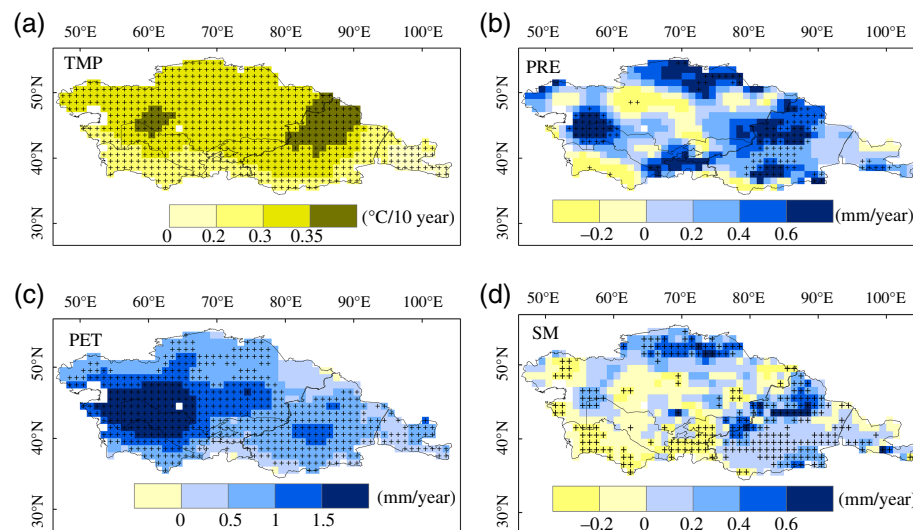
FIGURE 6 Spatial distributions of the linear trends of the TMP (a), PRE (b), PET (c) and SM (d) during the period of 1950–2015. Statistically significant linear trends at the 95% confidence level are indicated by cross ($p < .05$) [Colour figure can be viewed at wileyonlinelibrary.com]

between the drought indices and TMP, PRE, PET and SM are provided in sections 3.3 and 3.5, respectively.

3.3 | Relationships between the six drought indices and the TMP, PRE and PET

Five of the six drought indices are functions of TMP, PRE and PET. The major drivers of the different drought indices may be different. Further, drought conditions over different regions can be dominated by different drivers because of the differences in the regional climate variations. Therefore, in what follows we estimate CC between the drought indices and the three climatic factors including TMP, PRE and PET over the three regions (CASNW, CAS5 and NW), with the aim to identify major drivers of the drought conditions over the different regions.

As anticipated, SPI is significantly correlated with the PRE with the largest CC over CASNW (0.82), CAS5 (0.61) and NW (0.48) at the 99% confidence level, respectively (Table 4). TMP and PET have different influences on SPI over the three regions, especially for NW with the significant positive CC (0.28) between TMP and SPI, and negative CC (−0.21) between PET and SPI. Because PRE is the only input for calculating SPI, the relationship between TMP/PET on SPI should be explained by the interactions between TMP/PET and PRE. The positive influences of TMP on SPI may be caused by the conversion of casual link of the interaction between precipitation and temperature over the three regions which is consistent with the result in He *et al.* (2015). Although PET based on Penman–Monteith formula is mostly determined by TMP, PET calculation considers

more hydrological processes and parameters. As shown in Figure 3, TMP and PET obtain similar increasing trends but different inter-annual variations, which may be a possible reason to explain their different correlations with SPI. Because the PET was included in SPEI, very strongly significantly negative correlations are obtained over the three regions with the CC values −0.84 for CASNW, −0.83 for CAS5 and −76 for NW ($p < .01$). Although the effects of TMP on SPEI are weaker than these of PET, significant correlations between TMP and SPEI are also obtained over CASNW (CC = −0.46, $p < .01$), CAS5 (CC = −0.42, $p < .01$) and NW (CC = −0.40, $p < .01$) (Table 4).

In terms of the four PDSIs, they are negatively correlated with TMP over the three regions, with the strong impacts over CASNW and CAS5 (Table 4). As the similar correlations of PRE and PET with SPI and SPEI, PRE have the significantly positive correlations with the four PDSIs over the three regions with the largest CC in PDSI_pm than the other three PDSIs ($p < .01$). It is obvious that PET still has the significantly negative correlations with PDSIs which are stronger than TMP. It should be noted that all the climate factors (i.e., TMP, PRE and PET) have strongly significant influences on SPEI and PDSIs over CASNW and CAS5, whereas PRE and PET impact the above drought indices over NW. In addition, PRE have the dominant influences on all the indices but SPEI which is strongly affected by PET (Table 4). The above analysis indicates that the three climate factors control the drought variations over CAS5 while PRE and PET are the major factors on the drought over NE. The difference influences of the TMP on the drought indices between the CAS5 and NW may be caused by the insignificant increase of PRE in CAS5 and the significant increase of PRE in NW (Table S3). Spatial distributions of the CC values between the six drought indices and the three climatic factors are provided in Figures 7–9 for TMP, PRE and PET, respectively. The positive CC values between TMP and SPI are mainly distributed in part of west and south of CAS5 and most areas of NW with the significant CC in west and north of Kazakhstan, most of Tajikistan, and central and southern Xinjiang (Figure 7a). While the negative CC values mainly appear in the central and part northeastern Kazakhstan, almost regions of Turkmenistan and small part of Kunlun Mountain. Furthermore, only less than 6% areas have the significant CC values between TMP and SPI which are mainly distributed in northern Turkmenistan and western Kunlun Mountain (Figure 7a).

For SPEI, nearly all the study areas have the negative CC values which is caused by the temperature induced in SPEI (Figure 7b). More than 74% areas have the significant correlations ($p < .05$) between SPEI and TMP with the negative centres in the Areal Sea basin and central and part southern Xinjiang. The CC values between the four PDSIs and TMP have the similar spatial distributions (Figure 7c,f). In particular, the negative CC values account for 85, 70,

TABLE 4 Correlation coefficient (CC) results between climate factors (TMP, PRE and PET) and drought indices during 1950–2015. * indicates the CC is significant at the 95% confidence level ($p < 0.05$), and ** indicates the CC is significant at the 99% confidence level ($p < 0.01$)

Study area	Drought indices	TMP	PRE	PET
CASNW	SPI	0.12	0.82**	−0.45**
	SPEI	−0.46**	0.58**	−0.84**
	PDSI_pm	−0.25*	0.85**	−0.70**
	sc_PDSI_pm	−0.21	0.68**	−0.61**
	PDSI_th	−0.28*	0.78**	−0.74**
	sc_PDSI_th	−0.22	0.63**	−0.64**
CAS5	SPI	0.04	0.80**	−0.52**
	SPEI	−0.42**	0.61**	−0.83**
	PDSI_pm	−0.33**	0.85**	−0.77**
	sc_PDSI_pm	−0.26*	0.70**	−0.68**
	PDSI_th	−0.32*	0.76**	−0.77**
	sc_PDSI_th	−0.27*	0.63**	−0.67**
NW	SPI	0.28*	0.72**	−0.21
	SPEI	−0.40**	0.48**	−0.76**
	PDSI_pm	−0.06	0.81**	−0.56**
	sc_PDSI_pm	−0.04	0.62**	−0.42**
	PDSI_th	−0.06	0.83**	−0.60**
	sc_PDSI_th	0.02	0.68**	−0.43**

87 and 76% for PDSI_pm, sc_PDSI_pm, PDSI_th and sc_PDSI_th (Table S4). The corresponding significant negative CC values ($p < .05$) account for larger than 30% areas with their distributions mainly in central, southern and north-eastern Kazakhstan, most areas of Areal Sea Bain (Table S4 and Figure 7e,f).

The six drought indices are significantly positive correlated with PRE nearly over the whole regions which indicates the strong influences of PRE on the drought in CASNW (Figure 8). For the correlations of the drought indices and PET, most areas show the significantly negative CC values (Figure 9). The strong negative influences of PET on SPI are displayed excluding the weak negative and positive CC values in part of southwestern Kazakhstan, northwestern Uzbekistan and large part of southern Xinjiang (Figure 9a). The significantly negative correlations of SPEI and PET are distributed over all the areas with the centres in Areal Sea basin (Table S4 and Figure 9b). The four PDSIs still have the similar CC spatial distributions with the insignificant CC values in part of central and southern Xinjiang (Figure 9c,f). The areas with the significant negative CC values reach 93, 81, 100 and 86% for PDSI_pm, sc_PDSI_pm, PDSI_th and sc_PDSI_th (Table S4).

The above analyses clearly demonstrate that the major drivers have distinctive regional characteristics. Particularly, a drying CAS5 and a wetting NW were mainly caused by the combined effects of similar warming trends in TMP but larger increasing trend of PRE in NW than that of CAS5, and smaller increasing trend of PET in NW than CAS5 (Table S3). Moreover, the drying trend over central Kazakhstan was to a large extent controlled by the increased PET and decreased PRE; the enhanced droughts over Uzbekistan and Turkmenistan were dictated by the increased TMP and decreased PRE.

3.4 | Relationships between the drought indices and ENSO

Significantly positive correlation coefficients ($p < .05$ or $p < .01$) are obtained between the six drought indices (excluding SPEI with CC = 0.15) and Niños3.4 (Table 5), which show that ENSO has strong impacts on the wet and dry variations over the arid regions of central Asia. The largest correlation coefficient is for PDSI_pm (CC = 0.34, $p < .01$), followed by SPI (CC = 0.31, $p < .05$) and sc_PDSI_pm (CC = 0.31, $p < .05$). This result reveals that during El Niño, wetting over CASNW appears as over the southwestern United States–Mexican region, Argentina, East Africa and central Eurasia, which are opposite to the drying over the South Asia–Australia region, southern Africa and northern South America (Dai, 2011a). When the La Niña phases appear, it is drying over CASNW. For CAS5, the drought indices are associated with ENSO strongly, while they are weakly correlated with ENSO over NW according to the CC values in Table 5. Because the PRE has positive impacts on
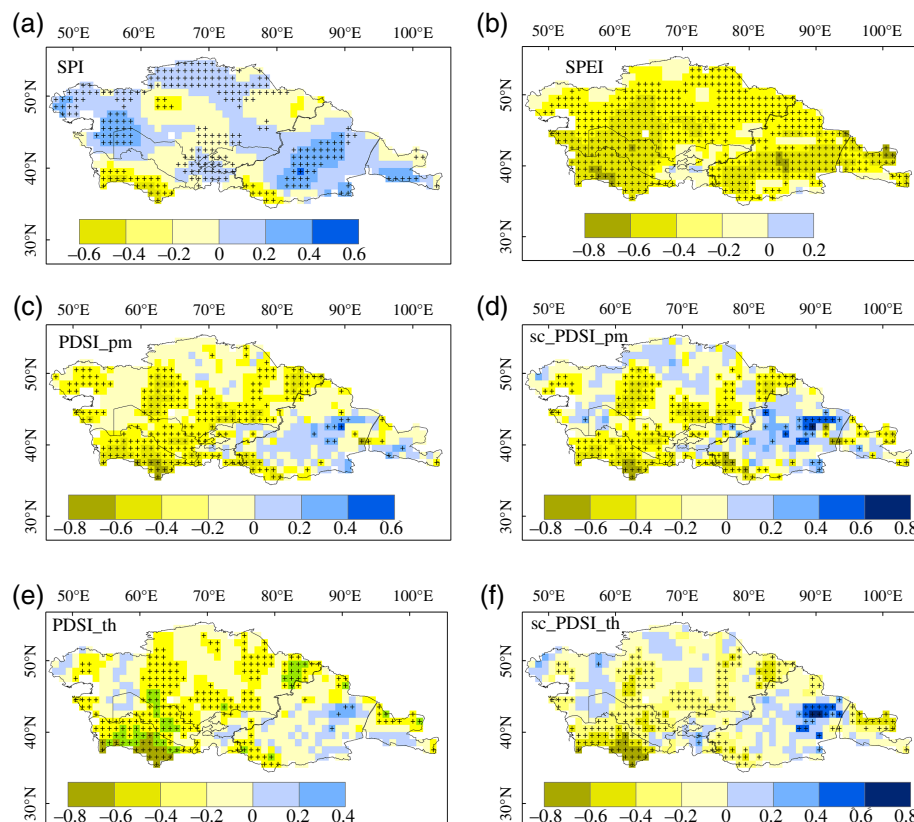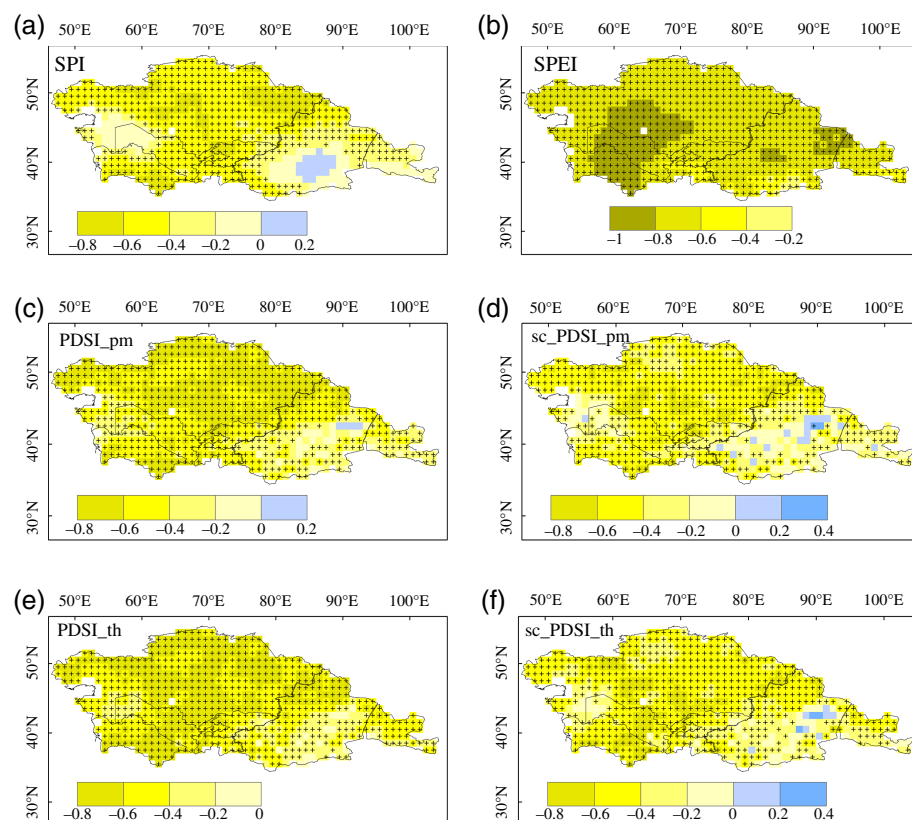

FIGURE 7 Correlation coefficients CC between TMP and annual drought indices during 1950–2015. Statistically significant CCs at the 95% confidence level are indicated by cross ($p < .05$) [Colour figure can be viewed at wileyonlinelibrary.com]
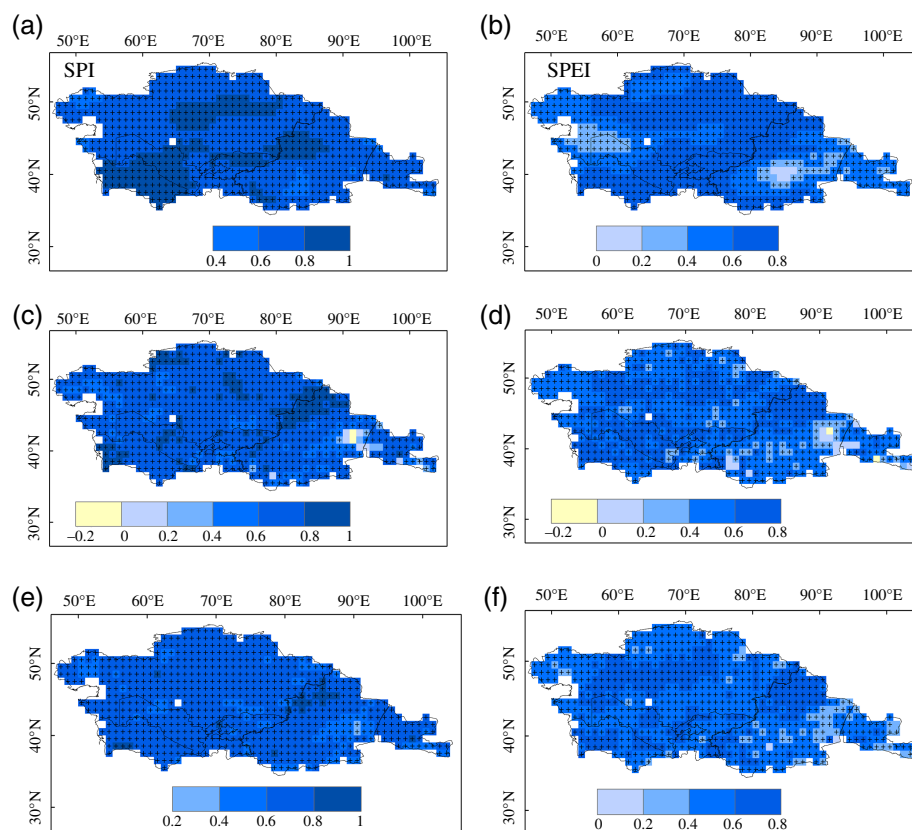
FIGURE 8 Correlation coefficients CC between PRE and annual drought indices during 1950–2015. Statistically significant CCs at the 95% confidence level are indicated by cross ($p < .05$) [Colour figure can be viewed at wileyonlinelibrary.com]

FIGURE 9 Correlation coefficients CC between PET and annual drought indices during 1950–2015. Statistically significant CCs at the 95% confidence level are indicated by cross ($p < .05$) [Colour figure can be viewed at wileyonlinelibrary.com]

the drought indexes according to the PCC results (Table 4), the positive influence of ENSO on the drought indexes may be caused by the remarkably positive relationship between ENSO and PRE over central Asia (please refer to Hu *et al.*, 2017, fig. 9; Chen *et al.*, 2018, table 5). The corresponding physical mechanisms about the impacts of ENSO on precipitation have been comprehensively analysed based on composite analysis and atmospheric circulation, which can be helpful to understand the relationships between ENSO and drought indices (Chen *et al.*, 2018).

The impact of ENSO on droughts has been identified, especially in the lags in some regions (e.g., Australia and Indonesia) (Vicente-Serrano *et al.*, 2011). Therefore, the lag correlations between the drought indices and ENSO are also identified. For the maximum correlation, 1-year lag (lag1) is detected from the CC values over the entire study area, especially in NW (Table 5). The time lag indicates that the impact of ENSO on the droughts could be lasted more than 1 year, which are same as in Sahel (Vicente-Serrano *et al.*, 2011). The 1-year lag detected in this study may help forecasting dry conditions in some regions (especially NW) up to 1 year before their occurrences. The time lag influence of ENSO on the drought indices are mainly caused by the time lag relationship between ENSO and precipitation (Chen *et al.*, 2018).

3.5 | Atmospheric circulation response to ENSO

The above analysis indicates that the significantly positive correlations are detected between ENSO and the drought indices. However, the physical mechanisms associated with the influence of ENSO on the drought variations of central Asia are still unclear. Therefore, composite analysis of drought indices, geopotential height (HGT) at 850 and 200 hPa levels and the corresponding wind fields using El Niño minus La Niña years are conducted to discuss the possible dynamical processes during 1950–2012. In this study, the El Niño year is defined when the Niño3.4 are not smaller than 1 SD and the La Niña year is defined as Niño3.4 $\leq$ $-SD$ (Hu *et al.*, 2017; Chen *et al.*, 2018). The geopotential height data and wind data are applied from the National Centers for Environmental Prediction (NCEP)/National Center for Atmospheric Research (NCAR) Reanalysis Monthly

Means and Other Derived Variables with a spatial resolution of $2.5 \times 2.5°$ for the period 1948 to present (https://www.esrl.noaa.gov/psd/data/gridded/data.ncep.reanalysis.derived.pressure.html; Kalnay *et al.*, 1996).

Since the PDSI_pm has the largest CC (0.34) with ENSO than the other drought indices, it is applied to make the composite analysis based on ENSO events. During El Niño, it is much wetter than the normal ENSO and La Niña over most parts of CASNW (about 93% areas), especially CAS5 (Figure 10). Furthermore, more than 78% areas with the positive anomalies are significant at 95% confidence level which may be caused by the more precipitation during the El Niño years. The areas with the negative anomalies are mainly distributed in part of Xinjiang and Hexi Corridor (Figure 10).

Comparing with La Niña, most of the low-latitude region south of 40°N and Europe are dominated by significantly anomalous high pressure with three high-pressure centres about (50°N, 15°E), (20°N, 15°E) and (40°N, 90°E) when El Niño occurs. Meanwhile, most of the low-latitude region north of 40°N is characterized with low-pressure anomalies (Figure 11a). Such atmospheric circulation pattern enhances the westerly and southwesterly (Figure 11b) and thus is favourable for transporting large amount of water vapour from the North Atlantic Ocean and Indian Ocean to central Asia (Wang *et al.*, 2014; Hu *et al.*, 2017; Chen *et al.*, 2018). That is, the southwestern and western water vapour path for central Asia reinforces during El Niños.

For the upper troposphere (Figure 11c,d), the significantly anomalous high pressure mainly appears at the south of 20°N and a low-pressure trough is existed around the eastern Mediterranean Sea and the northern Caspain Sea which is benefit to their water vapour transporting to the western and southwestern central Asia (most areas of CAS5). These results are consistent with the result in Mariotti (2007). Moreover, the more precipitation over most of CAS5 caused by the large amount water vapour from westerly and southwesterly (Hu *et al.*, 2017) results in the much wet in this region which explains the significant correlations between the drought indices in CAS5 and ENSO (Table 5). For NW, the weak correlations can be well explained by the less precipitation in El Niño.

TABLE 5 Correlation coefficient (CC) between SM, Niño3.4 and the drought indices for the period of 1950–2015, where the values in the brackets are the CC results about the 1-year lag (lag 1) between Niño3.4 and the drought indices. * indicates significant at a 95% confidence level ($p < 0.05$) and **indicates significant at a 99% confidence level ($p < 0.01$)

Study areas	Drought indices	SPI	SPEI	PDSI_pm	sc_PDSI_pm	PDSI_th	sc_PDSI_th
CASNW	Niño3.4	0.31* (0.62**)	0.15 (0.48**)	0.34** (0.45**)	0.31* (0.46**)	0.28** (0.49**)	0.27* (0.47**)
CAS5		0.35** (0.56**)	0.19 (0.44**)	0.38** (0.39**)	0.33** (0.42**)	0.29* (0.44**)	0.28* (0.42**)
NW		0.09 (0.48**)	0.003 (0.43**)	0.15 (0.42**)	0.14 (0.37**)	0.12 (0.49**)	0.14 (0.43**)
CASNW	SM	0.80**	0.59**	0.72**	0.64**	0.71**	0.60**
CAS5		0.81**	0.68**	0.74**	0.70**	0.73**	0.64**
NW		0.79**	0.37**	0.71**	0.62**	0.76**	0.69**

Composite result of PDSI_pm
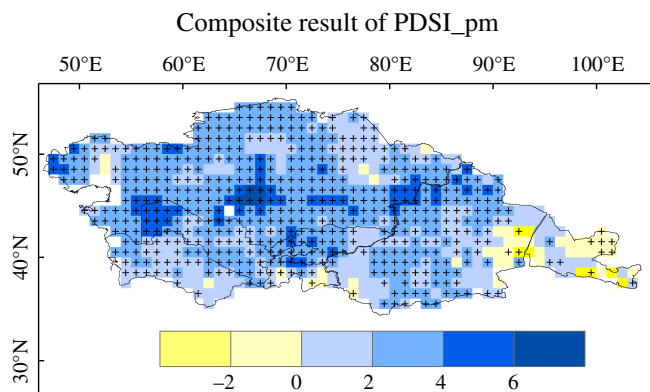
FIGURE 10 The El Niño minus La Niña composite difference in annual PDSI_m during 1950–2012, where the cross symbols are the different values significantly at the 95% confidence level ($p < .05$) [Colour figure can be viewed at wileyonlinelibrary.com]

3.6 | Connections between the drought indices and the SM

In this section, we explore the relationships between the drought indices and the estimated SM over the arid regions of central Asia to detect whether they have the same variabilities in the drought monitoring. The strongly significant correlations between the drought indices and SM are obtained (Table 5). Among the six drought indices, SPI has the largest correlation (CC = 0.80) with SM, and SPEI has the smallest value (CC = 0.59). Further, the two PDSIs have higher correlations with the SM than the two sc_PDSIs over the entire study area, respectively (PDSI_pm vs. sc_PDSI_pm: 0.72 vs. 0.64; PDSI_th vs. sc_PDSI_th: 0.71 vs. 0.60) which is

similar to the results for China (Wang *et al.*, 2015). The six drought indices are able to reasonably represent the SM (Table 5) over both CAS5 and NW. Particularly, the opposite linear trends of the SM are observed with a significantly increasing trend over NW (0.17 mm/year) and a decreasing trend over CAS5 (−0.018 mm/year), which confirms the wetting trend in NW and the drying trend in CAS5 from the agriculture drought perspective.

With the similar spatial patterns of the CC values between the six drought indices and SM, more than 90% areas have the significantly positive correlations at the 95% confidence level (100, 97, 97, 95, 99 and 97% for SPI, SPEI, PDSI_pm, sc_PDSI_pm, PDSI_th and sc_PDSI_th, respectively) (Figure 12). For SPI, the strong correlations (CC > 0.75) appears in most areas of Kazakhstan and Turkmenistan, northern Xinjiang, parts of Tarim Basin and western Heixi Corridor (Figure 10a). The areas with CC bigger than 0.75 of the five drought indices are obviously smaller than SPI (Figure 12). They have the same areas with the CC smaller than 0.50 in eastern and southeastern Xinjiang and small part area of the northern Kazakhstan (Figure 12b,f), which indicates that in these regions the drought indices have poor agreement with the SM than the other regions.

The above results suggest that the SM can be characterized well by the commonly used drought indices over most areas of CASNW which are similar with the conclusions as SPI in North Carolina (Sims *et al.*, 2002), SPEI in China (Wang *et al.*, 2015) and PDSI in the Great Hungarian Plain (Mika *et al.*, 2005) and in most areas of the former Soviet Union (42°–60°N, 27°–
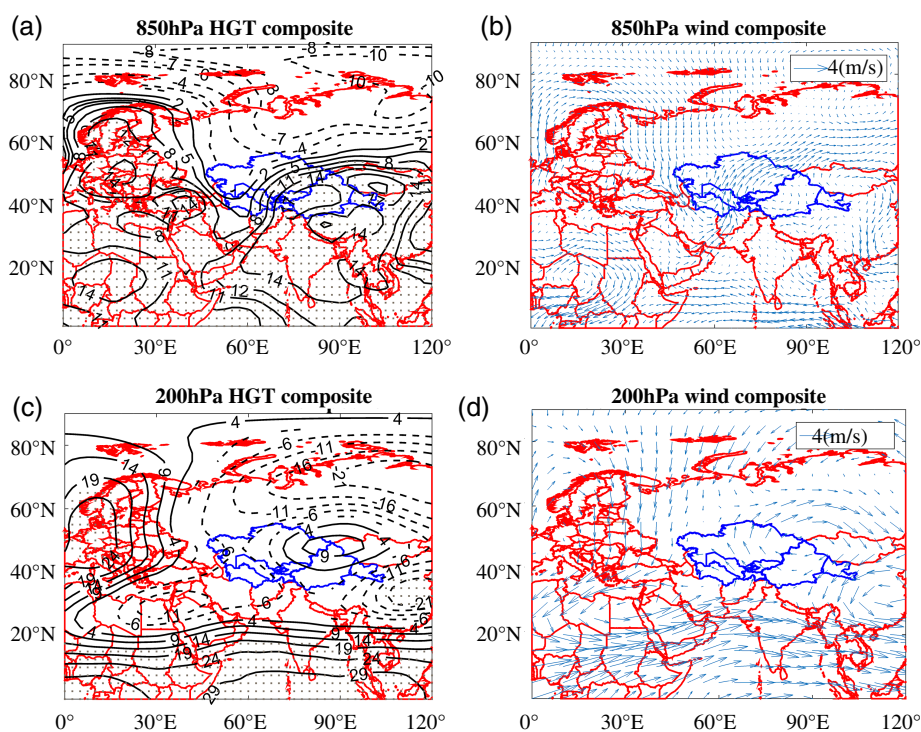
FIGURE 11 ENSO-based composites of geopotential height (HGT) (left column) and wind fields (right column) at 850 hPa (a, b) and 200 hPa (c, d) during 1950–2012. The contour intervals are 3 and 2 m for HGT at 850 and 200 hPa levels, respectively. The grey areas denote regions significant at the 95% level ($p < .05$) by the Student's *t* test. The zero contour is omitted, and dashed lines are negative [Colour figure can be viewed at wileyonlinelibrary.com]
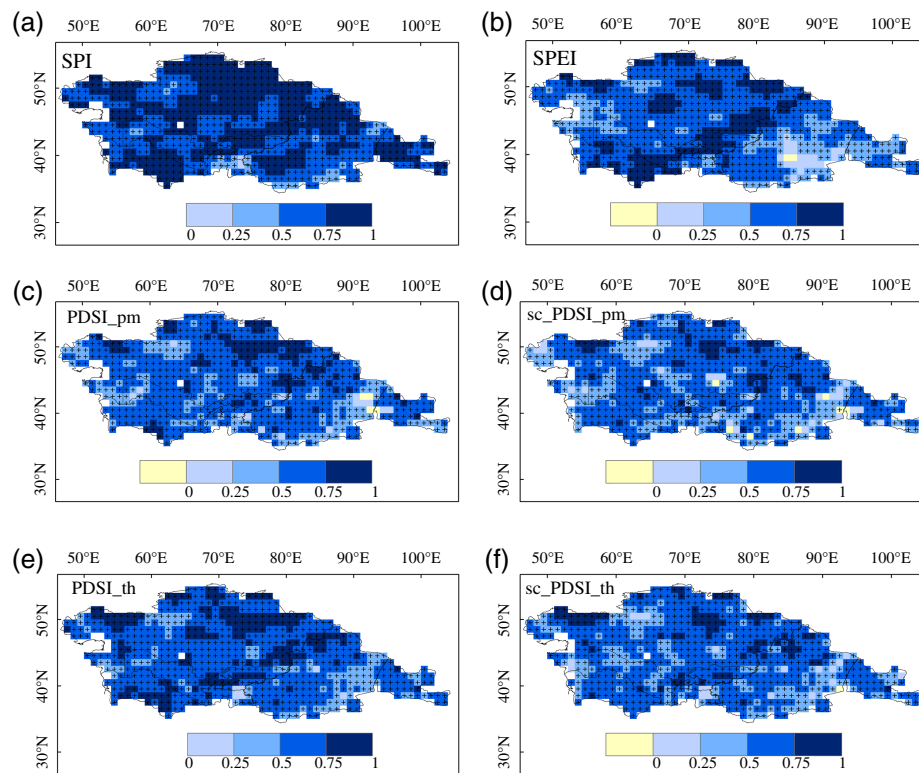
FIGURE 12 Correlation results between the drought indices and soil moisture (SM) during 1950–2015. Statistically significant CCs at the 95% confidence level are indicated by cross ($p < .05$) [Colour figure can be viewed at wileyonlinelibrary.com]

100°E; Dai *et al*., 2004). Their potentially abilities as indicators of SM may be caused by their own advantages: well representing the precipitation of SPI (Sims *et al*., 2002), considering both the influences of temperature, wind, solar radiation and humidity of SPEI (Wang *et al*., 2015), and using a water balance model with two-layer bucket-type of the soil moisture of PDSI (Palmer, 1965). Wang *et al*. (2015) suggested that the drought indices have different performances in characterizing SM at different soil layers. In addition, soil bulk density and soil organic carbon density have large influences on the spatial variations of the soil moisture-drought indices relationship. However, the SM data used in this study only considers one layer. The relationships between the drought indices and the SM will be discussed at different timescales, different layers over the regions with different soil types in a further study.

4 | DISCUSSION

Under global warming, the assessments of dry and wet variations have large uncertainties because of the complex hydroclimatological conditions over the different regions over the globe. Then, only single variable data set in hydroclimatological conditions cannot comprehensively reveal regional dry and wet changes (Greve *et al*., 2014). Based on the precipitation variations, DGDWGW was put forward in previous literatures (Allan *et al*., 2010; Chou *et al*., 2013). While this DGDWGW pattern does not hold over the global land or different regions (Greve *et al*., 2014; Feng and

Zhang, 2015). In order to examine the DGDWGW patterns over regions, in this study, six drought indices are applied to detect the dry and wet changes over CASNW.

Our results show that the opposite drying and wetting trends revealed by SPI and SPEI are resulted from their different inputs: only precipitation in SPI (Hao and Singh, 2015), while precipitation and PET in SPEI (Dai, 2011a). In fact, SPI and SPEI have the similar variabilities before the mid-1990s, after that time a sharp decreasing is found for SPEI which is caused by the significant increase of the PET. This indicates that the precipitation and PET only cannot realistically represent the dry and wet conditions over CASNW under global warming, and the dry and wet variations revealed by SPEI should be taken with caution. Including even more sophisticated treatment of water balances in the considering of radiation, wind and soil heat flux, PDSI seems to be a relatively better drought index in identifying the dry and wet variations over CASNW. The weak drying trend of CASNW revealed by the PDSI is consistent with the drying trend for the global land areas over the last century (Dai, 2013) (Table 6) and the period of 1950–2008 (Sheffield *et al*., 2012) (Table 6).

The drying trend in CAS5 and wetting trend in NW together with the previous studies (Greve *et al*., 2014; Feng and Zhang, 2015) indicate that the well accepted DGDWGW paradigm (Allan *et al*., 2010; Chou *et al*., 2013) is not valid over the study area. Because of the importance of regional dryness changes for society and ecosystem, studies on dry and wet variations should be relied on multiple hydro-

TABLE 6 Comparisons of the drought indices variations over arid regions of central Asia (CASNW) during 1950–2015 in this study to the results in other studies, PDSIARTS based on leaf area index-based total evapotranspiration (ARTS E0). PDSIAI based on the PET from Allen (1998)

Studies	Study areas	Study period	Data	Major conclusions
Dai (2013)	Globe	1923–2010	sc_PDSI_pm and CMIP	Increasing drought obtained by observations and models, being severe and widespread in next 30–90 yeas
Sheffield et al. (2012)	Globe	1950–2008	PDSI_th, PDSI_pm	−0.037 ±0.004/year for PDSI_th, −0.018±0.005/year for PDSI_pm, little change in global drought
Allan et al. (2010)	Tropic	1979–2008	Global Precipitation Climatology Project (GPCP)	DGDWGW pattern based on satellite data and climate models
Chou et al. (2013)	Globe	1979–2010	Precipitation	Wet seasons have become wetter; dry seasons have become drier
Greve et al. (2014)	Globe	1984–2005	Precipitation, evapotranspiration and PET	About three-quarters of the global land robust dryness changes cannot be detected. Only 10.8% global land has DGDWGW pattern
Feng and Zhang (2015)	Globe	1979–2013	SM	30% of global land has experienced robust moisture trends; only 15.12% of the land areas have followed the DGDWGW pattern
Chen et al. (2017)	China	1961–2012	Precipitation, SPEI, four PDSIs	Robust drying and wetting trends are found in different regions, and northwest of China with the wetting trend
Yan et al. (2016)	China	1982–2011	PDSI$_{ARTS}$, PDSI_th and PDSI_pm from 571 meteorological stations	No significant change of drought by PDSI$_{ARTS}$; PDSI_th and PDSI_pm overestimated drying trend
Zhai et al. (2010)	10 large regions of China	1961–2005	PDSI and SPI from 483 meteorological stations	PDSI and SPI can describe the tendency of dryness and wetness. Upward dry trends for three northeastern basins, upward wet trend for northwest region
Our study	CASNW	1950–2015	SPI, SPEI and the four PDSIs	Drying trend in CAS5 and wetting trend in NW. 3–7-year periods obtained for all the drought indices

climatological variables. Furthermore, the wetting trends over NW identified in this study are similar with previous studies based on the precipitation changes during the past five decades (Zhai et al., 2010; Chen et al., 2017) and the recent three decades (Yan et al., 2016).

In terms of the driving factors of dry and wet variations, our finding indicates that the major drought drivers have regional features: TMP, PRE and PET for CAS5, and PRE and PET for NW based on the CC result. Specifically, the increase in drought is attributed due to the nonsignificant increased PRE and significantly increased TMP and PET for CAS5. The increased drought over CAS5 increases the occurrence of the natural hazards and induces the exacerbation of the ecosystem, such as the decreasing of the vegetation, the desertification of the soil and the shrinking area of the Areal Sea (Lioubimtseva and Henebry, 2009; Chen, 2012). For NW, although the temperature is increased significantly as that of CAS5, the magnitude of the increased PET only accounts for 63% less than that of CAS5 which may be caused by the declining of the wind speed in NW (Shi et al., 2015). With the significantly increasing of PRE, NW has been experienced a wetting climatology since 1950s which is agreement with the climate transformation from warm-dry to warm-wet proposed by Shi et al (2007). This warm-wet climatology in NW is beneficial to the vegetation recovery of the desert ecosystem, the utilization of the water resource and the sustainable development of the society.

It is known that ENSO has significantly impacted on the recent drying by changing the temperature, precipitation, evaporation and atmospheric circulation (Dai, 2011b). Our result also shows that the dry and wet variations over CASNW are moderately correlated with the ENSO change

which is consistent with the positive influence of ENSO on the precipitation (Hu et al., 2017; Chen et al., 2018). Nevertheless, the interaction between the land surfaces (land use and land cover change) and the atmosphere plays a key role on the drying trends in arid regions (Wang et al., 2010), such as the bare soil reducing the net radiation at the surface and changing the drier and warmer conditions. A recent study (Yuan et al., 2017) suggested that land surface had impact on the local temperature and evaporation over central Asia. Therefore, these factors related to human activities should be considered in the physical mechanism analysis about the dry and wet variations.

5 | CONCLUSION

To address the "dry gets drier, wet gets wetter" (DGDWGW) paradigm, a case study over the arid regions of central Asia (CASNW) during 1950–2015 is conducted using six different drought indices: SPI, SPEI, PDSI_th, PDSI_pm, sc_PDSI_th and sc_PDSI_pm. The temporal characteristics and spatial distributions of the drought indices are studied by linear trend and nonlinear EEMD. The major driving factors of the droughts are detected by the PCC values with the three climatic variables: TMP, PRE and PET. The correlations between the six drought indices and other related variable (e.g., terrestrial water storage and SM) are analysed. Finally, the relationships between the drought indices and ENSO are explored by the correlation coefficient method. The major conclusions are following.

1. Although the six drought indices have similar inter-annual variations over CASNW during 1950–2015, the long-term trends are different. In particular, SPI and

SPEI can display different sign of trends and they can show same or opposite sign of trends compared with the four PDSIs which show similar trends. This demonstrates the limitations of SPI and SPEI as reliable indicators for drought trends because precipitation only is considered in SPI and PRE-PET is considered in SPEI. The four PDSIs confirm that CAS5 has a drying trend while NW has a wetting tendency, which indicates that the well accepted DGDWGW paradigm is not valid over the study area. The difference of signs of trends in drought indices further shows further complexity of wetting/drying trends at the regional level.

2. The nonlinear characteristics of the wet and dry variations are presented by the 3–7 years periods of all the six drought indices. More consistent spatial patterns can be found for the four PDSIs than for SPI and SPEI, which confirms the strength of the four PDSIs in realistically describing drought conditions over the study region. They show a wetting trend across north and central Xinjiang, and a drying trend in parts of central Kazakhstan, Uzbekistan and Turkmenistan. Further, the major drought drivers have regional features: with PRE and PET for CAS5 and PRE for NW.

3. A strong correlation between all the six drought indices and the estimated SM on the inter-annual scale was detected over the entire study area. Long term changes in the SM confirms the drying in CAS5 and wetting in NW.

4. ENSO has a strong influence on the drought variations represented by the significant correlations between Niño 3.4 and the drought indices. During El Niños, large amount of water vapour from the North Atlantic Ocean and Indian Ocean to central Asia are carried in central Asia by the westerly and southwesterly. In addition, a maximum 1-year lag correlation between the two was found (drought variations lags behind ENSO), which provides some potential for drought forecasting over the arid regions of central Asia, especially over NW.

ORCID

Zengyun Hu https://orcid.org/0000-0002-4259-9141
Xi Chen https://orcid.org/0000-0002-9569-728x
Deliang Chen https://orcid.org/0000-0003-0288-5618
Jianfeng Li https://orcid.org/0000-0002-9288-3415
Shuo Wang https://orcid.org/0000-0001-7827-187X
Qiming Zhou https://orcid.org/0000-0003-0934-0602

REFERENCES

Allan, R.P., Soden, B.J., John, V.O., Ingram, W. and Good, P. (2010) Current changes in tropical precipitation. *Environmental Research Letters*, 5, 025205.

Allen, R.G. (1998) *Crop Evapotranspiration: Guidelines for Computing Crop Water Requirements*. Rome: Food and Agriculture Organization of the United Nations.

Cayan, D., Das, T., Pierce, D., Barnett, T., Tyree, M. and Gershunov, A. (2010) Future dryness in the southwest US and the hydrology of the early 21st century drought. *Proceedings of the National Academy of Sciences of the United States of America*, 107, 21271–21276.

Chen, X. (2012) *Retrieval and Analysis of Evapotranspiration in Central Areas of Asia*. Beijing: China Meteorological Press (in Chinese).

Chen, D. and Chen, H. (2013) Using the Köppen classification to quantify climate variation and change: an example for 1901–2010. *Environmental Development*, 6, 69–79.

Chen, X. and Zhou, Q. (2015) *Ecological and Environmental Remote Sensing in Arid Zone: A Case Study of Central Asia*. Beijing: Science Press, pp. 4–5.

Chen, D., Gao, G., Xu, C., Guo, J. and Ren, G. (2005) Comparison of the Thornthwaite method and pan data with the standard Penman–Monteith estimates of reference evapotranspiration in China. *Climate Research*, 28, 123–132.

Chen, T., Zhang, H. and Chen, X. (2017) Robust drying and wetting trends found in regions over China based on Köppen climate classifications. *Journal of Geophysical Research: Atmospheres*, 122, 4228–4237. https://doi.org/10.1002/2016JD026168.

Chen, X., Wang, S. and Hu, Z. (2018) Spatiotemporal characteristics of seasonal precipitation and their relationships with ENSO in central Asia during 1901–2013. *Journal of Geographical Sciences*, 28, 1341–1368.

Cheng, S. and Huang, J. (2016) Enhanced soil moisture drying in transitional regions under a warming climate. *Journal of Geophysical Research: Atmospheres*, 121, 2542–2555.

Chou, C., Chiang, J., Lan, C., Chung, C., Liao, Y. and Lee, C. (2013) Increase in the range between wet and dry season precipitation. *Nature Geoscience*, 6, 263–267.

Dai, A. (2011a) Characteristics and trends in various forms of the Palmer drought severity index during 1900–2008. *Journal of Geophysical Research*, 116, D12115.

Dai, A. (2011b) Drought under global warming: a review. *Wiley Interdisciplinary Reviews: Climate Change*, 2, 45–65.

Dai, A. (2013) Increasing drought under global warming in observations and models. *Nature Climate Change*, 3, 52–58.

Dai, A., Trenberth, K. and Qian, T. (2004) A global dataset of Palmer drought severity index for 1870–2002: relationship with soil moisture and effects of surface warming. *Journal of Hydrometeorology*, 5, 1117–1130.

Fan, Y. and Dool, H. (2004) Climate Prediction Center global monthly soil moisture data set at 0.5 resolution for 1948 to present. *Journal of Geophysical Research*, 109, D10102.

Feng, H. and Zhang, M. (2015) Global land moisture trends: drier in dry and wetter in wet over land. *Scientific Reports*, 5, 18018. https://doi.org/10.1038/srep18018.

Franzke, C. (2012) Nonlinear trends, long-range dependence, and climate noise properties of surface temperature. *Journal of Climate*, 25, 4172–4183.

Gong, L., Xu, C.-Y., Chen, D. and Halldin, S. (2006) Sensitivity of the Penman–Monteith reference evapotranspiration to key climatic variables in the Changjiang (Yangtze River) basin. *Journal of Hydrology*, 329, 620–629.

Greve, P., Orlowsky, B., Mueller, B., Sheffield, J., Reichstein, M. and Seneviratne, S.I. (2014) Global assessment of trends in wetting and drying over land. *Nature Geoscience*, 7, 716–721. https://doi.org/10.1038/NGEO2247.

Guttman, N. (1998) Comparing the Palmer drought index and the standardized precipitation index. *Journal of the American Water Resources Association*, 34, 113–121.

Hao, Z. and Singh, V. (2015) Drought characterization from a multivariate perspective: a review. *Journal of Hydrology*, 527, 668–678.

Harris, I., Jones, P., Osborn, T. and Lister, D. (2014) Updated high-resolution grids of monthly climatic observations—the CRU TS 3.10 dataset. *International Journal of Climatology*, 34, 623–642.

He, B., Wang, H., Wang, Q. and Di, Z. (2015) A quantitative assessment of the relationship between precipitation deficits and air temperature variations. *Journal of Geophysical Research: Atmospheres*, 120, 5951–5961.

Hobbins, M., Dai, A., Roderick, M. and Farquhar, G. (2008) Revisiting potential evapotranspiration parameterizations as drivers of long-term water balance trends. *Geophysical Research Letters*, 35, L12403.

Hu, Z. and Huang, B. (2009) Interferential impact of ENSO and PDO on dry and wet conditions in the U.S. Great Plains. *Journal of Climate*, 22, 6047–6065.

Hu, Z., Zhang, C., Hu, Q. and Tian, H. (2014) Temperature changes in central Asia from 1979–2011 based on multiple datasets. *Journal of Climate*, 27, 1143–1167.

Hu, Z., Hu, Q., Zhang, C., Chen, X. and Li, Q. (2016a) Evaluation of reanalysis, spatially-interpolated and satellite remotely-sensed precipitation datasets in central Asia. *Journal of Geophysical Research: Atmospheres*, 121, 5648–5663.

Hu, Z., Li, Q., Chen, X., Teng, Z., Chen, C., Yin, G. and Zhang, Y. (2016b) Climate changes in temperature and precipitation extremes in an alpine grassland of central Asia. *Theoretical and Applied Climatology*, 126, 519–531.

Hu, Z., Zhou, Q., Chen, X., Qian, C., Wang, S. and Li, J. (2017) Variations and changes of annual precipitation in central Asia over the last century. *International Journal of Climatology*, 37, 157–170.

Hu, Z., Zhou, Q., Chen, X., Li, J., Li, Q., Chen, D., Liu, W. and Yin, G. (2018) Evaluation of three global gridded precipitation datasets in central Asia based on rain gauge observations. *International Journal of Climatology*, 9, 3475–3493.

Ji, F., Wu, Z., Huang, J. and Chassignet, E. (2014) Evolution of land surface air temperature trend. *Nature Climate Change*, 4, 462–466.

Kalnay, E., Kanamitsu, M., Kistler, R., Collins, W., Deaven, D., Gandin, L., Iredell, M., Saha, S., White, G., Woollen, J., Zhu, Y., Chelliah, M., Ebisuzaki, W., Higgins, W., Janowiak, J., Mo, K., Ropelewski, C., Wang, J., Leetmaa, A., Reynolds, R., Jenne, R. and Joseph, D. (1996) The NCEP/NCAR 40-year reanalysis project. *Bulletin of the American Meteorological Society*, 77, 437–470.

Lesk, C., Rowhani, P. and Ramankutty, N. (2016) Influence of extreme weather disasters on global crop production. *Nature*, 529, 84–87.

Li, Z., Chen, Y., Fang, G. and Li, Y. (2017) Multivariate assessment and attribution of droughts in central Asia. *Scientific Reports*, 7, 1316.

Lioubimtseva, E. and Cole, R. (2006). Uncertainties of climate change in arid environments of central Asia. *Reviews in Fisheries Science*, 14, 9–49.

Lioubimtseva, E. and Henebry, G. (2009). Climate and environmental change in arid Central Asia: Impacts, vulnerability, and adaptations. *Journal of Arid Environments*, 73, 963–977.

Mariotti, A. (2007) How ENSO impacts precipitation in southwest central Asia. *Geophysical Research Letters*, 34, L16706.

McKee, T.B., Doesken, N.J. and Kleist, J. (1993) The relationship of drought frequency and duration to time scales. In: *Eighth Conference on Applied Climatology*. Anaheim, CA: American Meteorological Society, pp. 179–184.

Mika, J., Horvath, S., Makra, L. and Dunkel, Z. (2005) The Palmer drought severity index (PDSI) as an indicator of soil moisture. *Physics and Chemistry of the Earth*, 30, 223–230. https://doi.org/10.1016/j.pce.2004.08.036.

Muirhead, R. (1982) *Aspects of Multivariate Statistical Theory*. Hoboken, New Jersey: John Wiley, pp. 187–189.

Nicholson, S., Leposo, D., Grist, J. (2001) The relationship between El Niño and drought over Botswana. *Journal of Climate*, 14, 323–335.

Palmer, W. (1965) *Meteorological Drought*, Vol. 45. Washington, DC: Office of Climatology Research Paper, Weather Bureau, 58 pp.

Qian, C., Fu, C. and Wu, Z. (2011) Changes in the amplitude of the temperature annual cycle in China and their implication for climate change research. *Journal of Climate*, 24, 5292–5302.

Schiemann, R., Chiemann, L., Luthi, D., Vidale, P. L. and Schar, C. (2008) The precipitation climate of central Asia—Intercomparison of observational and numerical data sources in a remote semiarid region. *International Journal of Climatology*, 28, 295–314.

Schrier, G., Jones, P. and Briffa, K. (2011) The sensitivity of the PDSI to the Thornthwaite and Penman–Monteith parameterizations for potential evapotranspiration. *Journal of Geophysical Research*, 116, D03106.

Seneviratne, S.I., Corti, T., Davin, E.L., Hirschi, M., Jaeger, E.B., Lehner, I., Orlowsky, B. and Teuling, A.J. (2010) Investigating soil moisture–climate interactions in a changing climate: a review. *Earth-Science Reviews*, 99, 125–161.

Sheffield, J., Wood, E. and Roderick, M. (2012) Little change in global drought over the past 60 years. *Nature*, 491, 435–438.

Sheffield, J. and Wood, E. (2008). Global Trends and Variability in Soil Moisture and Drought Characteristics, 1950–2000, from Observation-Driven Simulations of the Terrestrial Hydrologic Cycle. *Journal of Climate*, 21, 432–458.

Shi, P., Zhang, G., Kong, F. and Ye, Q. (2015) Wind speed change regionalization in China (1961–2012). *Advances in Climate Change Research*, 6, 151–158.

Sims, A., Niyogi, D. and Raman, S. (2002) Adopting drought indices for estimating soil moisture: a North Carolina case study. *Geophysical Research Letters*, 29, 1183.

Thornthwaite, C. (1948). An approach toward a rational classification of climate. *Geographical Review*, 38, 55–94.

Trenberth, K., Dai, A., Schrier, G., Jones, P., Barichivich, J., Briffa, K. and Sheffield, J. (2014) Global warming and changes in drought. *Nature Climate Change*, 4, 17–22.

Tucker, C., Pinzon, J., Brown, M., Slayback, D., Pak, E., Mahoney, R., Vermote, E. and Saleous, N. (2005) An extended AVHRR 8-km NDVI data set compatible with MODIS and SPOT vegetation NDVI data. *International Journal of Remote Sensing*, 26, 4485–5598.

Vicente-Serrano, S., Beguería, S. and López-Moreno, J. (2010) A multiscalar drought index sensitive to global warming: the standardized precipitation evapotranspiration index. *Journal of Climate*, 23, 1696–1718.

Vicente-Serrano, S.M., López-Moreno, J.I., Gimeno, L., Nieto, R., Morán-Tejeda, E., Lorenzo-Lacruz, J., Beguería, S. and Azorin-Molina, C. (2011) A multiscalar global evaluation of the impact of ENSO on droughts. *Journal of Geophysical Research*, 116, D20109.

Wang, G., Huang, J., Guo, W., Zuo, J., Wang, J., Bi, J., Huang, Z. and Shi, J. (2010) Observation analysis of land–atmosphere interactions over the Loess Plateau of northwest China. *Journal of Geophysical Research*, 115, D00K17.

Wang, S., Huang, J., He, Y. and Guan, Y. (2014) Combined effects of the Pacific Decadal Oscillation and El Niño–Southern Oscillation on global land dry–wet changes. *Scientific Reports*, 4, 6651.

Wang, H., Rogers, J. and Munroe, D. (2015) Commonly used drought indices as indicators of soil moisture in China. *Journal of Hydrometeorology*, 16, 1397–1408.

Wells, N., Goddard, S. and Hayes, M. (2004) A self-calibrating Palmer drought severity index. *Journal of Climate*, 17, 2335–2351.

Wu, Z. and Huang, N. (2004) A study of the characteristics of white noise using the empirical mode decomposition method. *Proceedings of the Royal Society of London A*, 460, 1597–1611.

Wu, Z. and Huang, N. (2009) Ensemble empirical mode decomposition: a noise-assisted data analysis method. *Advances in Adaptive Data Analysis*, 1, 1–41.

Yan, H., Wang, S., Wang, J., Lu, H., Guo, A., Zhu, Z., Myneni, R. and Shugart, H. (2016) Assessing spatiotemporal variation of drought in China and its impact on agriculture during 1982–2011 by using PDSI indices and agriculture drought survey data. *Journal of Geophysical Research: Atmospheres*, 121, 2283–2298.

Yin, Y., Ma, D., Wu, S., Dai, E., Zhu, Z. and Myneni, R.B. (2017) Nonlinear variations of forest leaf area index over China during 1982–2010 based on EEMD method. *International Journal of Biometeorology*, 61, 977–988.

Yuan, X., Wang, W., Cui, J., Meng, F., Kurban, A. and de Maeyer, P. (2017) Vegetation changes and land surface feedbacks drive shifts in local temperatures over central Asia. *Scientific Reports*, 7, 3287.

Zhai, J., Su, B., Krysanova, V., Vetter, T., Gao, C. and Jiang, T. (2010) Spatial variation and trends in PDSI and SPI indices and their relation to streamflow in 10 large regions of China. *Journal of Climate*, 23, 649–663.

Zhang, L., Cheng, L. and Brutsaert, W. (2017) Estimation of land surface evaporation using a generalized nonlinear complementary relationship. *Journal of Geophysical Research: Atmospheres*, 122, 1475–1478.

SUPPORTING INFORMATION

Additional supporting information may be found online in the Supporting Information section at the end of the article.